J Nanopart Res (2021) 23: 21
https://doi.org/10.1007/s11051-020-05123-y

RESEARCH PAPER

Effect of cross-linking and thermal budget on plasmonic sensing and sub-surface segregation of in situ synthesized gold in polymer nanocomposite

Srinivas Bathini · Duraichelvan Raju · Simona Badilescu · Muthukumaran Packirisamy

Received: 20 May 2020 / Accepted: 14 December 2020 / Published online: 4 January 2021

Abstract Surface gold–poly (dimethylsiloxane) nanocomposites are a special category of composites, with gold nanoparticles segregated in a polymer's sub-surface layer. In this work, sub-surface nanocomposites were created by the in situ synthesis of gold, by using the solution of a gold precursor. The in situ reduction of gold ions by the polymer's cross-linking agent (a vinyl silicon compound) and the subsequent diffusion of gold nanoparticles into the PDMS matrix through heat treatment are investigated, principally, by UV-Vis spectroscopy, scanning electron microscopy (SEM), atomic force microscopy (AFM), X-ray diffraction (XRD), and X-ray photoelectron spectroscopy (XPS). It is shown that the diffusion stabilizes the freshly formed gold nanoparticles into the sub-surface layer, where they form small aggregates. The kinetics of the in situ reduction reaction at the solution-film interface is studied. The interplay between the reduction of gold ions and the cross-linking agent's continuous diffusion toward the surface is also discussed in detail. Further, the effect of the sub-surface segregation of gold nanoparticles and their subsequent spatial distribution on the nanocomposite's sensing capability is discussed as well.

Keywords PDMS · Surface nanocomposites · In situ reduction · Sub-surface segregation · Sensor

S. Bathini · D. Raju · S. Badilescu · M. Packirisamy (✉)
Optical Bio-Microsystems Laboratory and Micro Nano Bio Integration Center, Department of Mechanical, Industrial and Aerospace Engineering, Concordia University, Montreal, Canada
e-mail: pmuthu@alcor.concordia.ca

Introduction

Nanoparticle-polymer composites are advanced functional materials, with nanoparticles integrated into a polymer matrix. Therefore, nanocomposites have the outstanding electrical, optical, and magnetic properties of their metal components in addition to the polymers' transparency and processability properties. Optical nonlinearities and infra-low/ultra-high refractive indices, suitable for ultrathin color filters, UV absorbers, tunable optical filters, optical sensors, waveguides, optical strain detectors, and thermochromic materials, are only some of the potential applications of nanocomposites that originate from the properties of nano-sized noble metals (Algorri et al. 2016; Beecroft and Ober 1997; Faupel et al. 2010; Caseri 2000, 2009; Carotenuto et al. 2006; Camargo et al. 2009; Althues et al. 2007; Li et al. 2010a). The design, fabrication, and characterization of conducting polydimethylsiloxane (PDMS) with metallic powder for microheaters and temperature sensors have also been reported (Chuang and Wereley 2009). Stretchable PDMS structures doped with gold nanoparticles have been prepared and suggested for strain sensors (Cataldi et al. 2012). Gold (Au) and silver (Ag), as well as their nanocomposites, have also been used for water purification, targeted drug release, antimicrobial coatings, antibiotics, analysis of environmental pollutants, and immunosensing experiments (Li et al. 2010b; Nicolais and Carotenuto 2014; Scott et al. 2010; De Jesús et al. 2004; Ahmadivand et al. 2019; Ahmadivand et al. 2020).

The gold and silver nanoparticles have strong localized surface plasmon resonance (LSPR) bands in the visible spectrum and their nanocomposites can also be

used for sensing applications. Generally, nanocomposites' biosensing properties depend on the parameter related to their preparing conditions, pivotal for the distribution of metal nanoparticles in the polymer matrix. Since the spatial distribution of (AuNPs) determines the biosensing properties, it is essential to develop mechanisms and methods to control it (Kumar and Krishnamoorti 2010).

Nanocomposites can be synthesized either by in situ methods in which a polymer reacts with a metal precursor to create nanoparticles or by ex situ methods, in which prefabricated nanoparticles are embedded into the polymer matrix. Besides, physical techniques such as chemical vapor deposition, ion implantation, and thermolysis were successfully used to prepare gold on the surface of the nanocomposites (Stepanov and Khaibullin 2004; Niklaus and Shea 2011).

In some cases, depending on the polymer's softening temperature, nanoparticles are embedded just below the polymer's surface, where they reach a metastable state with minimum Gibbs free energy (Kovacs and Vincett 1984). The limited movement of nanoparticles (from the surface to the sub-surface layer) is accounted for by the tendency to reduce their high surface energy. Despite the efforts to prepare nanocomposites with appropriate morphologies and enhanced surface properties, the control of nanoparticles' spatial distribution remains still at an emerging stage (Ramesh et al. 2009).

Generally, when nanoparticles are well-dispersed in the polymer matrix, the nanocomposite will have only the individual components additive properties in the absence of nanoparticle-nanoparticle interactions. But, if the polymer is structured, entirely new properties would emerge. For example, in PDMS's particular case with a segregated layer, nanoparticles are formed and concentrated in the segregated layer(s), and the new properties originate from their closeness (Giesfeldt et al. 2005). These special categories of nanocomposites, called surface nanocomposites, have a three-dimensional distribution of the AuNPs, and they were found suitable, mostly, for surface-enhanced Raman scattering (SERS) applications (Hasell et al. 2008; Bonyar et al. 2018; Bonyár et al. 2018; Firestone et al. 2015).

An ordered structural design, such as the segregated layer, can be used to control the degree of nanoparticle aggregation within the polymer in the case of PDMS. PDMS is a polymer used for the fabrication of microfluidic devices. It has received utmost attention due to its ease of preparation, low cost, good transparency, and non-toxicity to biomolecules.

The cross-linking of PDMS is obtained by hydrosilylation, where vinyl groups of one component (the pre-polymer) react with hydrosilane groups of the second component (the curing agent, a vinyl silicon compound) in a Pt-catalyzed reaction (Deshmukh and Composto 2007; Simpson et al. 2003) as shown in Eq. (1).

$$(\text{Cross}-\text{linker})-\text{Si}-\text{H} + \text{CH}_2 = \text{HC}-\text{Si}-(\text{polymer}) \xrightarrow[\text{heat}]{\text{Pt catalyst}} -\text{Si}-\text{CH}_2-\text{CH}_2-\text{Si}-(3\text{D network}) \quad (1)$$

Many authors (Batch et al. 1991; Simpson et al. 2004) have studied the kinetics of the hydrosilylation reaction catalyzed by a platinum complex but only for the case of bulk reaction between vinyl-terminated PDMS and silane cross-linkers. For thin films or coatings, the cross-linking reactions' kinetics is different from the bulk behavior because of segregation, either at the interface or the atmosphere or substrate. In this way, the migration toward the surface decreases the cross-linker and Pt catalyst concentration in bulk.

Zhang et al. and Goyal et al. have suggested that, in the case of in situ synthesis of gold, the curing agent's excess may act as a reducing agent of gold ions (Zhang et al. 2008; Goyal et al. 2009). Zhang investigated the effect of changing the curing (cross-linking) agent to monomer ratio (η), that is, the curing agent concentration. The optical and thermoplasmonic response of the in situ reduced AuNPs have been measured (Berry Jr et al. 2012), and various applications of the in situ prepared Au-PDMS nanocomposite have been reported (Ryu et al. 2011; Massaro et al. 2011).

Our group has systematically studied the in situ synthesis of gold and silver nanocomposites of PDMS, especially for microfluidic sensing applications (SadAbadi et al. 2012; Ozhikandathil et al. 2012; Badilescu and Packirisamy 2012; Fanous et al. 2018). To develop in situ nanocomposite for various applications, it is essential to systematically investigate the in situ surface nanocomposites prepared by reducing gold ions by the excess of cross-linking agents in thin self-standing PDMS films. In particular, we are interested in how (i) the cross-linking agent concentration influences the distribution and the in situ synthesis of gold nanoparticles after a specific synthesis time as shown in the schematic of Fig. 1a, and (ii) how the thermal budget drives the AuNPs from the sub-surface layers of the

polymer deeper as shown in the schematic of Fig. 1b. In the case of free-standing films, the precursor molecules' diffusion occurs simultaneously through all six sides of the sample. As the focus of this work is to find out the suitability of this nanocomposite for sensing applications, we were interested in the agglomeration state of AuNPs in the surface segregated layers and their diffusion into PDMS during the annealing process. This work represents an attempt to establish how the distribution of AuNPs affects the nanocomposite's sensing capability. The work is also pertinent to the general topic of the diffusion of nanoparticles in polymer films (coatings) and its effect on nanocomposites' properties.

Experimental

Materials

Gold (III) chloride trihydrate ($HAuCl_4.3H_2O$), isopropyl alcohol, dimethylformamide, chloroform, toluene, and anisole were purchased from Sigma-Aldrich. The Sylgard® 184 elastomer kit for the PDMS fabrication was purchased from Dow Corning. De-ionized (DI) water with a resistivity of 18 MΩ, used in all the experiments, was obtained from the NANO pure ultrapure water system (Barnstead). Ethanol was purchased from Fisher Chemicals.

Synthesis of the gold-PDMS nanocomposite

The gold precursor solution is prepared by dissolving gold (III) chloride trihydrate ($HAuCl_4.3H_2O$) in ethanol. The concentration of the precursor solution was 0.6% (wt/v). The PDMS samples were prepared with two concentrations of base to cross-linking agents, namely 4:1 and 10:1. For the synthesis of Au-PDMS nanocomposites, the prepared PDMS films were immersed vertically in the gold precursor solution and incubated for around 48 h. Figure 2a illustrates the immersed film in the precursor solution, and Fig. 2b shows the nanocomposite after the completion of the reaction (the PDMS film is shown slightly slanted for clarity). In the following sections, this nanocomposite will be referred to as an "as-prepared sample" (meaning the sample was taken out after a synthesis time of 48 h at room temperature and was not heat-treated (t_{synth} = 48 h, no heat treatment). After the in situ synthesis, the morphology of formed gold nanoparticles aggregates in the as-prepared sample is altered by heat treating the Au-PDMS nanocomposite samples at 200 °C for 30 min. These samples will be referred to as "heat-treated samples" (t_{synth} = 48 h, Temp = 200 °C, 30 min heat treatment).

Characterization methods

The Au-PDMS nanocomposites were characterized by UV-Visible spectroscopy, scanning electron microscopy (SEM), atomic force microscopy (AFM), X-ray diffraction (XRD), and X-ray photoelectron spectroscopy (XPS). For all the spectral measurements, Perkin Elmer lambda 650 UV-Visible spectrometer was used. The SEM images were captured using Hitachi S 3400N. AFM images were captured in tapping mode by scanning an area of 20 × 20 μm, using scanning probe microscopy. XRD measurements were obtained using a PANalytical X'Pert PRO system. XPS analysis was performed using a VG Scientific ESCALAB MKII spectrometer with Ar+ sputtering energy of 1 keV, and estimated sputtering rate of 3.4 nm/min on a surface area of 2 mm × 3 mm is sputtered and analyzed until to a depth without any gold signal. Also, the sensitivity of the synthesized nanocomposite for sensing was measured using solvents with different refractive indices. The sensitivity measurements were performed by measuring the nanocomposite samples absorption spectra after immersing them in a quartz cuvette, filled with the solvent, for 1 h.

Results and discussion

Assessment of the distribution of AuNPs

For visual analysis of the distribution of AuNPs after the in situ synthesis, a portion of the sample with a thickness of 1 mm was sliced, using a sharp blade. Out of the six faces of the sample, four were sliced, except the top and the bottom faces, as shown in the schematic of Fig. 2c.

Further, for a qualitative assessment of how AuNPs were distributed in the polymer matrix, the samples were cut as described in the experimental part. Figure 2d and e show the images of the sliced 1-mm Au-PDMS nanocomposites for both the as-prepared and heat-treated samples. The same qualitative assessment has been done for nanocomposites prepared with a higher concentration of the precursor as well, and the results were found to be the same. This confirmed that,

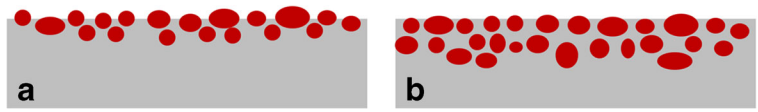

Fig. 1 Illustration of diffusion of gold nanoparticles and the effect of heat treatment on a nanocomposite sample: (**a**) Schematic showing AuNPs in the as-prepared sample. (**b**) Heat-treated sample (only the upper portion of the sample is shown for simplicity)

under the experiment's conditions, no matter the concentration of the gold precursor, nanoparticles are in situ formed and concentrated only at the interfaces. This qualitative observation prompted us to undertake a detailed investigation of Au-PDMS nanocomposites using various methods suitable for their characterization to quantify the influence of cross-linking agents and thermal budget.

In situ synthesis of AuNPs on the surface of the polymer

During the in situ synthesis, the precursor solution's gold ions are reduced to AuNPs by the excess of curing agent in PDMS. The amount of curing agent present in PDMS and the precursor solution's concentration will determine the rate of AuNPs formation. In other words, by increasing the amount of curing (cross-linking) agent in PDMS, by keeping the concentration of the precursor molecule constant, more AuNPs will be formed at the interface(s) of the polymer. Therefore, it is expected to have more gold ions reduced in 4:1 PDMS samples, where the reductant is in a higher concentration than in the 10:1 sample. In previous work, we have found that the in situ synthesis of nanoparticles in the PDMS matrix, using the ethanol solution for the precursor, is faster than in the aqueous solution (SadAbadi et al. 2013). This was accounted for by the high rate of permeation of the ethanol-based precursor solution. To study the kinetics of the reaction, the evolution of the absorption spectra of nanocomposites prepared in ethanol solution (0.6% wt/v) has been examined and shown in Fig. S1a, S1b.

$$3\ \begin{array}{c}|\\ \mathrm{Si}-\mathrm{H}\\ |\end{array} + \frac{3}{2}\mathrm{H_2O} + 2\mathrm{AuCl_4^-} \rightarrow \frac{3}{2} - \begin{array}{c}|\\ \mathrm{Si}-\mathrm{O}-\\ |\end{array}\begin{array}{c}|\\ \mathrm{Si}-\\ |\end{array} 2\mathrm{Au} + 8\mathrm{Cl^-} + 6\mathrm{H^+} \quad (2)$$

The reaction of the formation of gold nanoparticles is shown in Eq. (2). To better understand the kinetics of the in situ reduction, the variation of absorbance values of the Au LSPR bands at each time interval is shown in Fig. S1a, S1b. From these results, under the experiment's conditions, the reduction process seems to be completed after 80 h in the case of the 4:1 sample. More gold results when the curing agent's concentration is higher (4:1 samples).

The maximum absorbance of the Au LSPR band is shown against the time for the concentrations of cross-linking agents, namely 4:1 and 10:1. Figure 3a shows the three phases that describe kinetics' progress: induction, the actual formation step, and saturation. As shown in Fig. 3a, the induction step is around 5 h in both cases, while the actual formation step takes about 100 h in the case of the 4:1 sample and 140 h for the 10:1 sample. After this time, very few new gold nanoparticles are formed (saturation). The shorter time of saturation, in the case of the 4:1 ratio sample, is due to the higher reaction rate because of the relatively higher concentration of the reductant.

From the evolution of the AuNP's plasmonic band, it can be presumed that the precursor solution continues to enter the PDMS film, and the gold ions are reduced, forming AuNPs until the whole surface area is filled. After this, AuNPs start to aggregate inside the film, giving rise to a broad absorption peak in the UV-Visible spectrum. The Au LSPR band's broadening reflects the nanoparticles aggregated state, after around 100 h of reaction. The evolution of the aggregation of gold nanoparticles is shown in Fig. 3b. It can be seen that, in the case of the 4:1 sample, where the rate of the reduction is faster, the width of the band shows a steady increase, but this is not the case for the 10:1 sample, where the amount of the reductant is significantly lower.

Morphology of the Au-PDMS surface composites

The SEM images shown in Fig. 3c–h confirm that the gold nanoparticles start to aggregate as the synthesis progresses, in agreement with the evolution of the band's absorbance and width, as seen in Fig. 3a, b. Simultaneously, the formation of large aggregates is reflected in the widening of the absorption bands, as shown in the images. The SEM images of the 10:1 sample at 48 h and 96 h do not display any particles on the surface of PDMS, but at 216 h, a few

nanoparticles can be seen. From the images, it can be inferred that the rate of in situ synthesis is considerably lower in the 10:1 sample than in the 4:1 sample, as the amount of the reducing agent is less in the 10:1 sample. The SEM images confirm the formation of significantly more AuNPs in the samples prepared with a higher concentration of curing agent (4:1; Fig. 3c–e) compared to the (10:1; Fig. 3f–h) samples.

In previous work, we have prepared and characterized several gold-polymer surface nanocomposites (Massaro et al. 2011). Morphology investigations of these samples have revealed that as-prepared nanocomposites always had gold aggregates on the surface. The heat treatment, in general, reduced the size of the aggregates or even disaggregated them completely, releasing individual nanoparticles. To better observe nanoparticle aggregates morphological changes, AFM studies have been carried out on both the as-prepared and heat-treated nanocomposite samples of 10:1 and 4:1 composition. In the case of the in situ prepared Au-PDMS nanocomposites, by comparing the AFM images of as-prepared and heat-treated samples in Fig. 4a, b, it can be seen

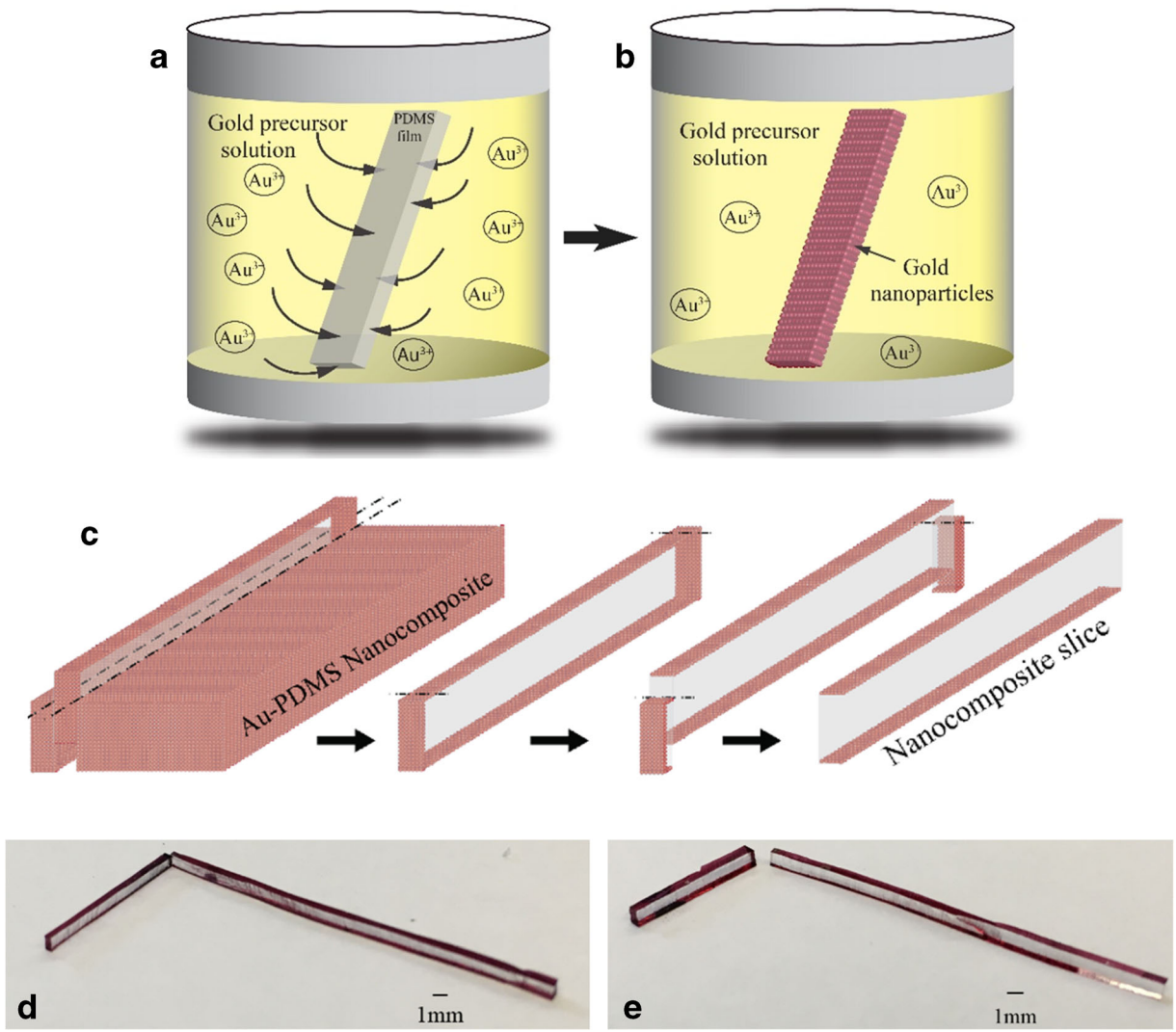

Fig. 2 In situ synthesis and slicing of the sample: (**a**) Schematic of in situ synthesis; the PDMS film, immersed in the gold precursor solution (**b**) Au-PDMS nanocomposite (red), after 48 h. (**c**) Schematic of slicing the Au-PDMS nanocomposite sample. (**d**) Image of sliced 1-mm-thick as-prepared sample. (**e**) Image of sliced 1-mm-thick heat-treated sample at 200 °C for 30 min

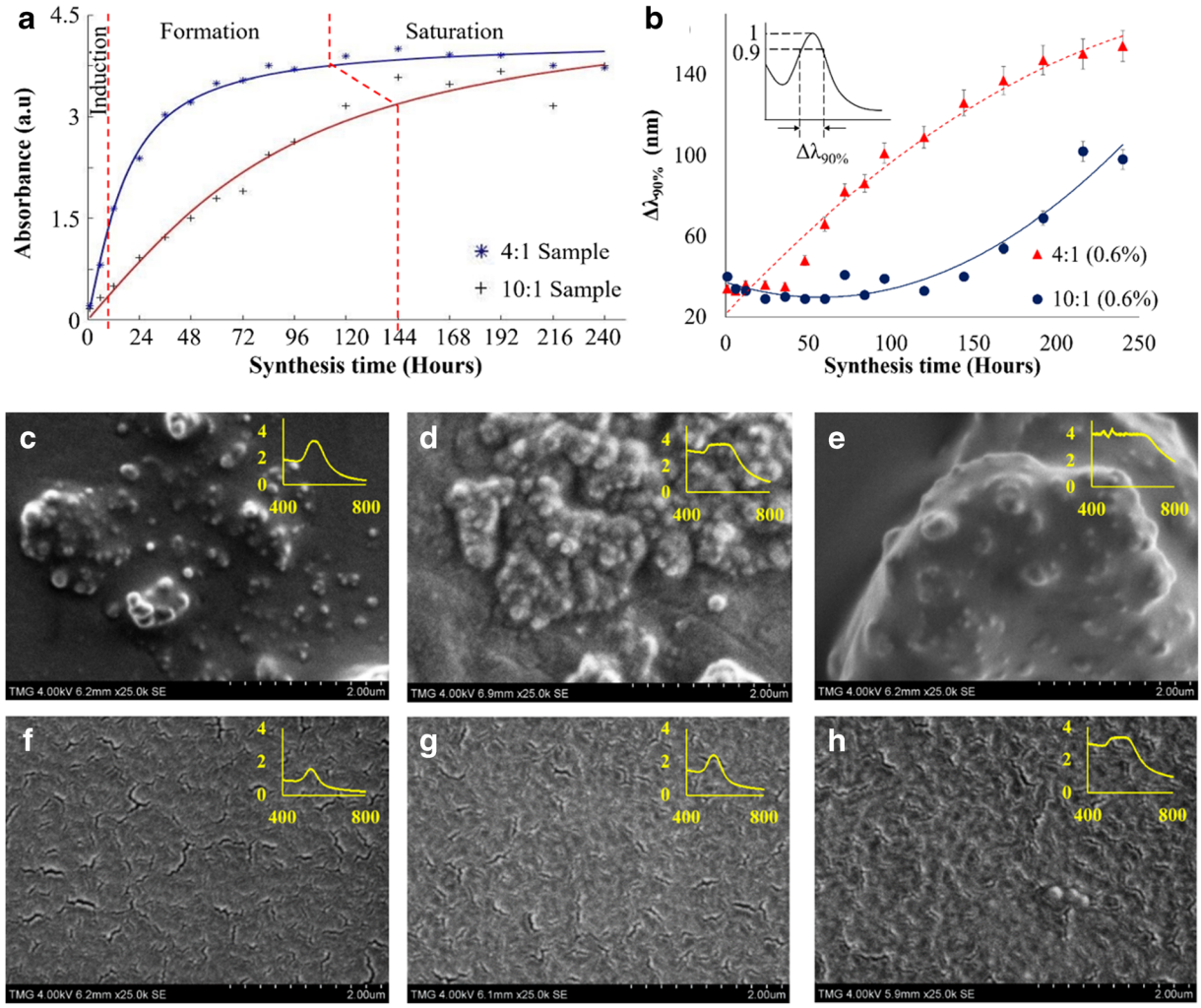

Fig. 3 Evolution of the in situ reduction reaction for two concentrations of the cross-linking agent: (**a**) Evolution of absorbance around 540 nm against synthesis time (t_{synth}). (**b**) The bandwidth measured at 90% of the spectral peak corresponding to two concentrations of the cross-linking agent. (**c**–**h**) SEM images of 1-mm-thick samples at different synthesis time, along with their absorption bands (inset) (images (**c**–**e**) 4:1 sample at 48 h, 96 h, and 216 h, and images (**f**–**h**) 10:1 sample at 48 h, 96 h, and 216 h, respectively)

that the aggregates are present on the surface and a complete disaggregation through the heat treatment process does not happen.

Figure 4a shows the phase contrast image with its topography image (inset) of 10:1 as-prepared aggregated samples with particle sizes ranging from hundreds of nanometers to several microns on the surface of the nanocomposite. The topography image clearly shows that the aggregates seem to be covered with a thin layer of PDMS. As the heat treatment process changes the morphology, the aggregates appear to be re-organized and distributed on the surface, as shown in Fig. 4b. Figure 4b shows the presence of smaller aggregates, even after the heat treatment. The same tendency, but with a higher amount of gold nanoparticles, is observed in the phase contrast and topography images of the 4:1 PDMS sample, as shown in Fig. 4c, d.

Sensitivity measurements of the platforms

The refractive index sensitivity of 1-mm-thick 10:1 and 4:1 nanocomposite sample for as-prepared treated and heat-treated at 200 °C was measured using various solvents as mentioned in the "Experimental" section. Figure 5 shows the corresponding sensitivity plots.

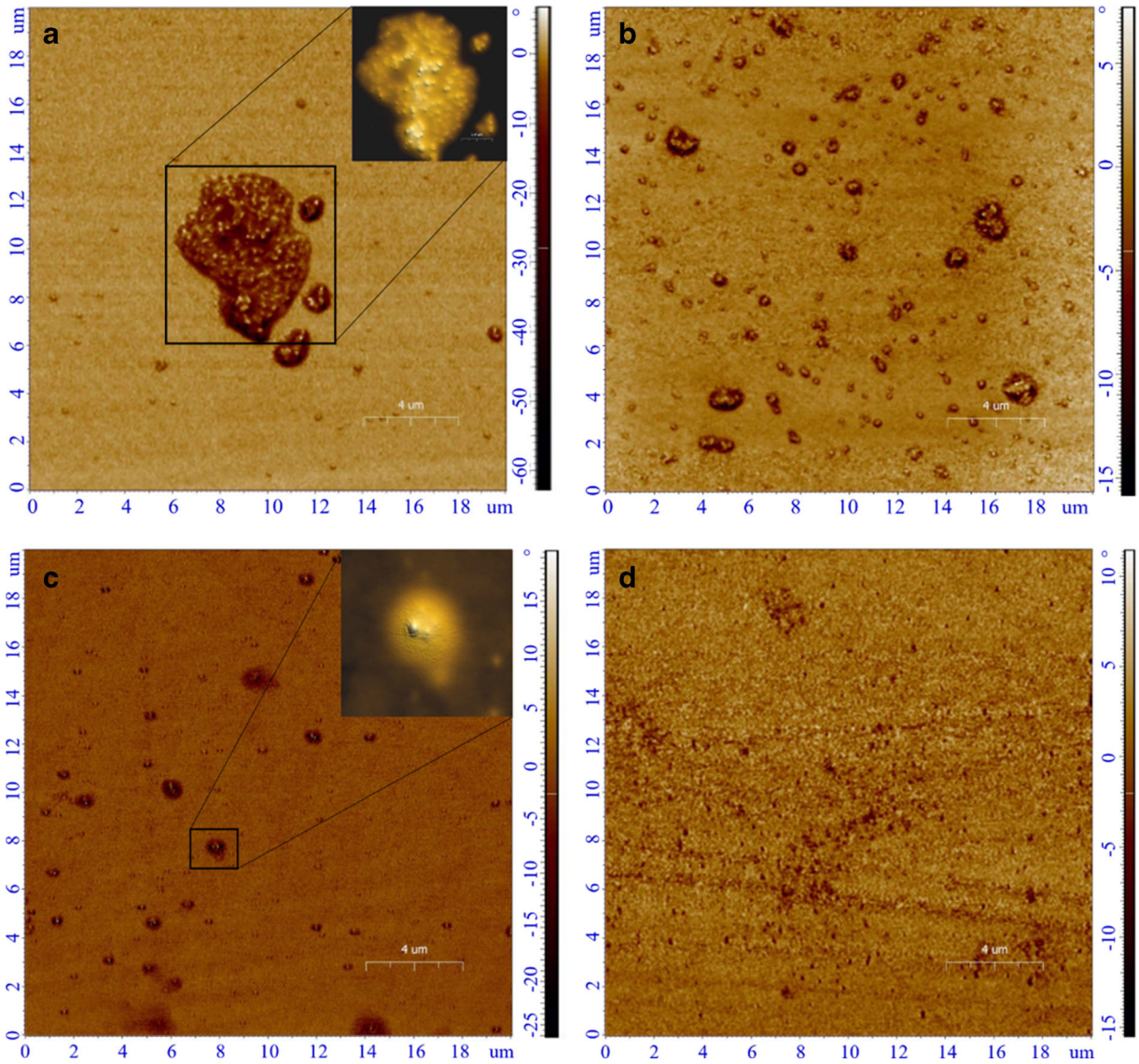

Fig. 4 AFM phase contrast images: (**a**–**b**) 10:1 as-prepared (t_{synth} = 48 h, no heat treatment) along with the topography image (inset) and heat-treated (t_{synth} = 48 h, T = 200 °C, 30 min heat treatment) PDMS sample (**c**–**d**) 4:1 as-prepared, along with the topography image (inset) and heat-treated PDMS sample

From the plots, it can be clearly seen that the sensitivity of all the nanocomposite platforms is relatively low.

The low refractive index sensitivity found for the Au-PDMS nanocomposite samples confirms the presence of most nanoparticles under the surface, covered by a thin polymer layer, as shown in the topography image (inset) of Fig. 4a, c, that is, not available for sensing while the gold nanoparticles, prepared by ex situ synthesis, or physical deposition methods such as chemical vapor deposition, ion implantation, and thermolysis are located on the surface of the film (Stepanov and Khaibullin 2004; Niklaus and Shea 2011). In contrast, in the case of in situ synthesis, the Au nanoparticles are submerged under the surface, surrounded by the polymer chains, and, therefore, are not in direct contact with the analyte. Even after heat treatment, when more nanoparticles diffuse into the polymer, there are no particles on the surface. This would explain the low sensitivity of the platform in the case of in situ synthesized Au NP. Furthermore, for this platform, the FoM has been calculated, and it is in the order of 13.31, 10.94 for 10:1 as-prepared, and heat-treated samples, respectively. In

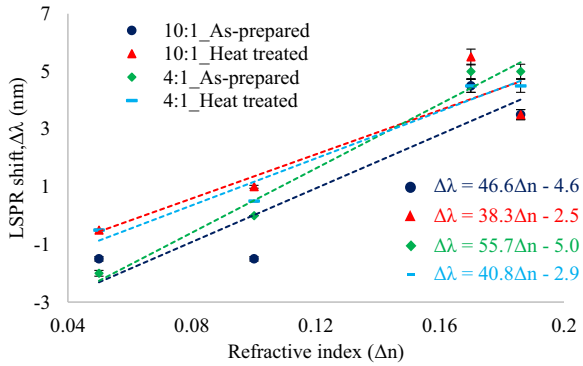

Fig. 5 Sensitivity measurements of a 1-mm-thick 10:1 and 4:1 nanocomposite sample, as-prepared (t_{synth} = 48 h, no heat treatment) and heat-treated (t_{synth} = 48 h, T = 200 °C, 30 min heat treatment) (n = 6)

contrast, for the 4:1 as-prepared and heat-treated samples, it is 11.14 and 9.06, respectively.

Distribution of AuNPs in the polymer film

The distribution of AuNPs in the depth of the Au-PDMS nanocomposite was analyzed by XPS. Figure 6a shows the elemental composition of the as-prepared ethanol nanocomposite sample (4:1 ratio), plotted against the binding energy of the corresponding atomic orbital. The distribution of AuNPs, along with the depth of the nanocomposite sample, was analyzed. The gold atomic percentage was plotted against the depth, as shown in Fig. 6b, c for the as-prepared and heat-treated samples, respectively.

It can be observed from the XPS analysis in Fig. 6b–d that most of the reduced gold nanoparticles are just below the surface layer, concentrated in a strip of around 100 nm, in the case of both as-prepared and heat-treated samples. However, gold at an atomic concentration of about 0.9% was found in the heat-treated 10:1 sample until a depth of around 1 μm while, in the case of the 4:1 sample, the concentration of gold, right under the surface, was found higher (about 3.5%) but decreased abruptly with depth. In the heat-treated sample, the strip of AuNPs is found deeper, and some more AuNPs can be seen in the sample's depth.

A part of the AuNPs has diffused to a depth of almost 700 nm in the as-prepared samples of 10:1 and 4:1 ratios and a depth of more than 1200 nm in the heat-treated samples of 10:1. The XPS measurements show that the morphology is changed when the samples are heat-treated at 200 °C (see the AFM images Fig. 4b, d). The aggregates become smaller, and the nanoparticles are redistributed over the surface and in depth. Figure 6d shows the schematic of the re-distribution of AuNPs and the gold atomic percentage in the sub-surface of the as-prepared and heat-treated samples with 10:1 and 4:1 composition.

The schematic shows the diffusion of AuNPs into the sample's depth when their kinetic energy is increased by heating. The schematic is a simplified view of diffusion from only the top of the sample. In reality, as AuNPs are formed at each interface of the free-standing sample, the diffusion is not unidirectional, and the trajectories of AuNPs may intersect with those of the particles in the vicinity, coming from the sides of the sample. The results show that the AuNPs from the sub-surface layers are redistributed upon heat treatment. It can be inferred that the curing agent in self-standing thin films is concentrated on the surfaces of the films (in contact with the atmosphere) and that the reduction reaction is taking place exclusively there and not inside the film.

To better understand the synthesis of AuNPs on the surface of the PDMS sample, a schematic of the in situ synthesis of AuNPs on the polymer's surface is shown in Fig. 7a–e. The excess of the free cross-linking agent migrates toward the interfaces and reduces the incoming gold precursor molecules. After the nucleation, the growth of AuNPs, and aggregates formation, the gold structure will embed in the polymer. Heat treating the nanocomposite sample at 200 °C for 30 min would drive more cross-linker molecules to the surface, and additional AuNPs will be formed at the interfaces.

When the nanocomposite's sensitivity is compared with the XPS results, it is very clear that the sensitivity of the nanocomposite depends on the amount of gold present in the sample. Table 1 shows the amount of gold synthesized represented by the area under the curves for the as-prepared and heat-treated samples of the composition 10:1 and 4:1. If the Au_{total} of 10:1 as-prepared is set as a reference, considering the curves from Fig. 6b, c and normalized to 100%, the process of heat treatment at 200 °C for 30 min results in the formation of more gold, that is, 2.06 times more than in the as-prepared sample. By analyzing the Au_{total} and the XPS curve pattern, it is clear that the heat treatment is not only increasing the amount of gold synthesized but it is also driving the gold nanoparticles deeper into the surface of the nanocomposite. For this reason, the sensitivity of the 10:1 heat-treated sample is reduced

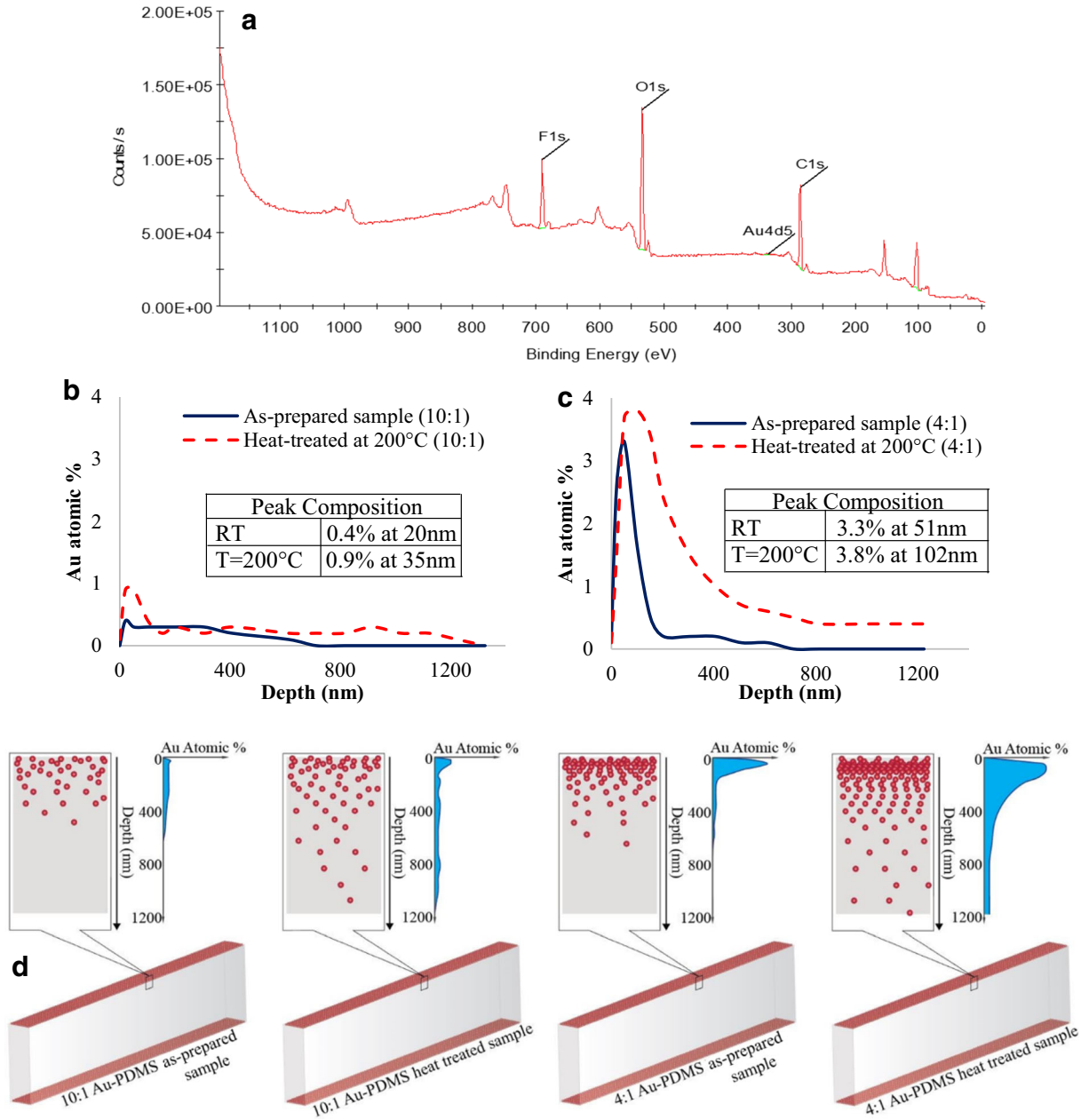

Fig. 6 Analysis of gold atomic percentage as a function of depth, in the case of as-prepared (t_{synth} = 48 h, no heat treatment) and heat-treated (t_{synth} = 48 h, Temp = 200 °C, 30 min heat treatment) samples: (**a**) XPS spectrum showing the elements present in the Au-PDMS nanocomposite, (**b**) 1-mm-thick 10:1 sample, (**c**) 1-mm-thick 4:1 sample. (**d**) Schematic showing the distribution of AuNPs and gold atomic percentage in the sub-surface of samples

when compared to the 10:1 as-prepared. A similar trend is observed in the case of the 4:1 as-prepared and heat-treated samples. Also, the normalized Au_{total} shows that the 4:1 as-prepared sample has a 2.52 times higher percentage of gold than that of the 10:1 as-prepared sample because of the higher amount of cross-linking agent present in the 4:1 sample. Thus, due to the higher percentage of gold in 4:1 as-prepared samples, the sensitivity is higher than the 10:1 as-prepared sample. Therefore, if a given application requires a higher sensitivity, the cross-linking agent to the PDMS base ratio has to be

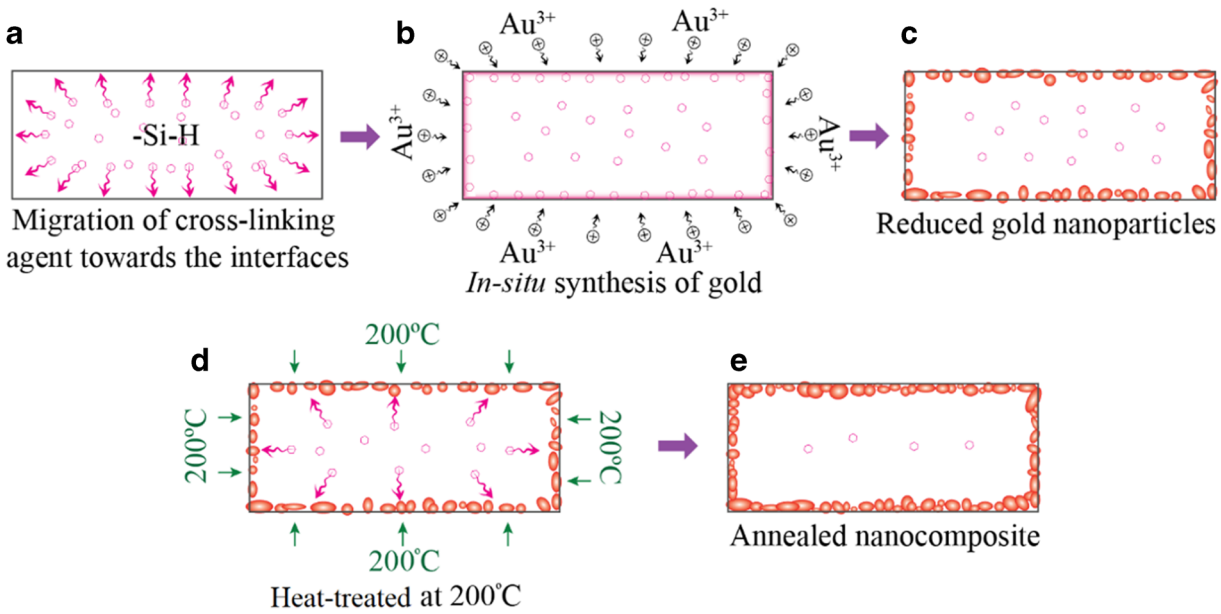

Fig. 7 Schematic of in situ formation, sinking, and re-distribution of AuNPs: (**a**) The excess of cross-linking agent migrates to the interfaces. (**b**) Reduction of gold ions (Au^{3+}). (**c**) In situ formed AuNPs sink under the surface. (**d**) New cross-linking molecules migrate toward the interfaces and reduce the remaining gold precursor molecules during heat treatment at 200 °C for 30 min. (**e**) A larger amount of (additional) AuNPs is formed in the sub-surface and some migrate inside the polymer due also to the migration of cross-linking agent during heat treatment

4:1 or more. If the application needs further distribution of nanoparticles in the nanocomposite, heat treatment could be considered as well.

In addition to sensing applications, Au(Ag)-PDMS nanocomposites, with the addition of carbon nanotubes, can be used for shielding from electromagnetic interference (Ozhikandathil et al. 2015; Raju et al. 2020).

Mechanism of formation of sub-surface segregated AuNPs

Unusual sub-surface structures, prepared by vacuum deposition onto heat or solvent vapor-softened thermoplastic polymer substrates, have been reported (Kovacs and Vincett 1982; Kovacs et al. 1983; Kovacs and Vincett 1983). For example, silver crystalline aggregates and other metal structures have been observed by SEM at a depth of several particles below the polymer surface. The detailed calculation of surface and interfacial tension forces demonstrated that the completely embedded sub-surface structures are thermodynamically the most stable. We hypothesized that the gold nanoparticles formed at the surface by in situ synthesis would also diffuse and completely embed in PDMS.

The surface free energy associated with a particle is:

$$F_s = A\,\gamma_1 \tag{3}$$

Table 1 Relation between the concentrations of cross-linker, the atomic percentage of synthesized gold, and their sensitivity

Nanocomposite sample type	Total gold synthesized (Au_{total} % * nm)	Normalized amount of gold (%)	Sensitivity (nm/RIU)
10:1 as-prepared sample (t_{synth} = 48 h, no heat treatment)	158.83	100	46.6
10:1 heat-treated sample (t_{synth} = 48 h, T = 200 °C, 30 min heat treatment)	327.10	206	38.3
4:1 as-prepared sample (t_{synth} = 48 h, no heat treatment)	400.63	252	55.7
4:1 heat-treated sample (t_{synth} = 48 h, T = 200 °C, 30 min heat treatment)	1374.52	865	40.8

t_{synth}, synthesis time; T, heat treatment temperature, Au_{total}, gold nanoparticles synthesized over 1200 nm in %

where γ_1 is the surface tension of the particle and A is its surface area.

When the particle is embedded, the surface free energy change will be:

$$\Delta F_s = A\,(\gamma_{12} - \gamma_1) \quad (4)$$

where γ_{12} is the interfacial tension and $A\gamma_{12}$ is the interfacial free energy.

Embedding is favorable, that is, $\Delta F_s < 0$ when the surface tension of the particle is larger than the interfacial free energy so that the sinking process will be energetically favorable.

The interfacial tension (γ_{12}) between PDMS and the gold nanoparticles has been reported to be around 4.0 mN/m (Borrell and Gong 2007). In comparison, the surface tension of AuNPs (γ_1) was calculated to be 8.78 N/m (Nanda et al. 2008) and $\gamma_1 = 6.3$ N/m for AuNP in a polymer matrix (Lamber et al. 1995). According to these data, the interfacial tension is inferior to the surface tension of the gold nanoparticles (weak Au-PDMS interactions), and consequently, the thermodynamic criterion for sinking is fulfilled.

Conclusions

The distribution of in situ prepared AuNPs on the surface of PDMS self-standing films has been investigated by SEM, AFM, XRD, XPS, and UV-Visible spectroscopy. It was found that nanoparticles are formed by in situ reduction of gold ions on the film's surface by the curing (cross-linking) agent, and, right after formation, they are segregated in the sub-surface layer of PDMS, and only a few nanoparticles in depth. The distribution pattern at room temperature and after heat treatment at 200 °C was studied with the curing agent's amount in the PDMS composition. It is inferred that in thin self-standing PDMS films, the excess of curing agent migrates toward the interfaces with the atmosphere and reduces the incoming gold ions. The influence of the amount and distribution of AuNPs in PDMS on the nanocomposite platform's refractive index sensitivity is discussed. The results show that the Au-PDMS surface nanocomposite film's sensing capability is low due to the polymer layer covering the AuNPs. The formation of the sub-surface structure in a thin self-standing nanocomposite film is accounted for by the weak Au-PDMS interfacial interactions, permitting the gold to sink under the surface and embed it in the polymer.

Supplementary Information The online version contains supplementary material available at https://doi.org/10.1007/s11051-020-05123-y.

Authors' contributions S.B. (Simona Badilescu) and M. Packirisamy conceived the study and experiments. S.B. (Srinivas Bathini) and D. Raju carried out experiments and contributed to the manuscript. All authors have contributed and reviewed the final manuscript.

Funding MP was financially supported from NSERC Discovery and Concordia Research Chair.Data availabilityNot applicable.

Compliance with ethical standards

Conflict of interest The authors declare that there are no conflicts of interest.

Code availability Not applicable.

References

Ahmadivand A, Gerislioglu B, Ramezani Z, Ghoreishi SA (2019) Attomolar detection of low-molecular weight antibiotics using midinfrared-resonant toroidal plasmonic metachip technology. Phys Rev Appl 12:3. https://doi.org/10.1103/PhysRevApplied.12.034018

Ahmadivand A, Gerislioglu B, Ahuja R, Mishra YK (2020) Terahertz plasmonics: the rise of toroidal metadevices towards immunobiosensing. Mater Today 32:108–130. https://doi.org/10.1016/j.mattod.2019.08.002

Algorri JF, Poudereux D, García-Cámara B, Urruchi V, Sánchez-Pena JM, Vergaz R, Caño-García M, Quintana X, Geday MA, Otón JM (2016) Metal nanoparticles-PDMS nanocomposites for tunable optical filters and sensors. Opt Data Process Storage 2:1–6. https://doi.org/10.1515/odps-2016-0001

Althues H, Henle J, Kaskel S (2007) Functional inorganic nanofillers for transparent polymers. Chem Soc Rev 36:1454–1465. https://doi.org/10.1039/b608177k

Badilescu S, Packirisamy M (2012) Microfluidics-nano-integration for synthesis and sensing. Polymers 4(2):1278–1310. https://doi.org/10.3390/polym4021278

Batch GL, Macosko CW, Kemp DN (1991) Reaction kinetics and injection molding of liquid silicone rubber. Rubber Chem Technol 64(2):218–233. https://doi.org/10.5254/1.3538554

Beecroft LL, Ober CK (1997) Nanocomposite materials for optical applications. Chem Mater 9(6):1302–1317. https://doi.org/10.1021/cm960441a

Berry KR Jr, Russell AG, Blake PA, Roper DK (2012) Gold nanoparticles reduced in situ and dispersed in polymer thin films: optical and thermal properties. Nanotechnology 23: 375703. https://doi.org/10.1088/0957-4484/23/37/375703

Bonyar A, Izsold Z, Himics L, Veres M, Csarnovics I (2018) Investigation of PDMS-gold nanoparticle composite films for plasmonic sensors. In: 2017 IEEE 23rd International Symposium for Design and Technology in Electronic Packaging, SIITME 2017 - Proceedings, pp 25–28. https://doi.org/10.1109/SIITME.2017.8259850

Bonyár A, Izsold Z, Borók A, Csarnovics I, Himics L, Veres M, Harsányi G (2018) PDMS-Au/Ag nanocomposite films as highly sensitive SERS substrates. Proceedings 2(13):1060. https://doi.org/10.3390/proceedings2131060

Borrell M, Gong Y (2007) Surface functionalized nanoparticles as surfactants. Proceeding of AIChE Annual meeting. https://www.aiche.org/conferences/aiche-annual-meeting/2007/proceeding/paper/128a-surface-functionalized-nanoparticles-surfactants

Camargo PHC, Satyanarayana KG, Wypych F (2009) Nanocomposites: synthesis, structure, properties and new application opportunities. Mater Res 12(1):1–39. https://doi.org/10.1590/S1516-14392009000100002

Carotenuto G, LaPeruta G, Nicolais L (2006) Thermo-chromic materials based on polymer-embedded silver clusters. Sensors Actuators B Chem 114(2):1092–1095. https://doi.org/10.1016/j.snb.2005.07.044

Caseri W (2000) Nanocomposites of polymers and metals or semiconductors: historical background and optical properties. Macromol Rapid Commun 21(11):705–722. https://doi.org/10.1002/1521-3927(20000701)21:11<705::AID-MARC705>3.0.CO;2-3

Caseri W (2009) Inorganic nanoparticles as optically effective additives for polymers. Chem Eng Commun 196(5):549–572. https://doi.org/10.1080/00986440802483954

Cataldi U, Cerminara P, DeSio L, Caputo R, Umeton CP (2012) Fabrication and characterization of stretchable PDMS structures doped with Au nanoparticles. Mol Cryst Liq Cryst 558(1):22–27. https://doi.org/10.1080/15421406.2011.653675

Chuang HS, Wereley S (2009) Design, fabrication and characterization of a conducting PDMS for microheaters and temperature sensors. J Micromech Microeng 19(4):1. https://doi.org/10.1088/0960-1317/19/4/045010

De Jesús MA, Giesfeldt KS, Sepaniak MJ (2004) Improving the analytical figures of merit of SERS for the analysis of model environmental pollutants. J Raman Spectrosc 35(10):895–904. https://doi.org/10.1002/jrs.1231

Deshmukh RD, Composto RJ (2007) Surface segregation and formation of silver nanoparticles created in situ in poly (methyl methacrylate) films. Chem Mater 19(4):745–754. https://doi.org/10.1021/cm062030s

Fanous M, Badilescu S, Packirisamy M (2018) Thermal manipulation of gold nanocomposites for microfluidic platform optimization. Plasmonics 13:305–313. https://doi.org/10.1007/s11468-017-0515-3

Faupel F, Zaporojtchenko V, Strunkus T, Elbahri M (2010) Metal polymer nanocomposites for functional applications. Adv Eng Mater 12(12):1177–1190. https://doi.org/10.1002/adem.201000231

Firestone MA, Hayden SC, Huber DL (2015) Greater than the sum: synergy and emergent properties in nanoparticle–polymer composites. MRS Bull 40(09):760–767. https://doi.org/10.1557/mrs.2015.202

Giesfeldt KS, Connatser RM, De Jesús MA, Dutta P, Sepaniak MJ (2005) Gold-polymer nanocomposites: studies of their optical properties and their potential as SERS substrates. J Raman Spectrosc 36(12):1134–1142. https://doi.org/10.1002/jrs.1418

Goyal A, Kumar A, Patra PK, Mahendra S, Tabatabaei S, Alvarez PJJ, John G, Ajayan PM (2009) In situ synthesis of metal nanoparticle embedded free standing multifunctional PDMS films. Macromol Rapid Commun 30(13):1116–1122. https://doi.org/10.1002/marc.200900174

Hasell T, Lagonigro L, Peacock AC, Yoda S, Brown PD, Sazio PJA, Howdle SM (2008) Silver nanoparticle impregnated polycarbonate substrates for surface enhanced Raman spectroscopy. Adv Funct Mater 18(8):1265–1271. https://doi.org/10.1002/adfm.200701429

Kovacs GJ, Vincett PS (1982) Formation and thermodynamic stability of a novel class of useful materials: close-packed monolayers of submicron monodisperse spheres just below a polymer surface. J Colloid Interface Sci 90(2):335–351. https://doi.org/10.1016/0021-9797(82)90302-2

Kovacs GJ, Vincett PS (1983) Subsurface particulate film formation in softenable substrates: present status and possible new applications. Thin Solid Films 100(4):341–353. https://doi.org/10.1016/0040-6090(83)90159-1

Kovacs GJ, Vincett PS (1984) Subsurface particle monolayer and film formation in softenable substrates: techniques and thermodynamic criteria. Thin Solid Films 111(1):65–81. https://doi.org/10.1016/0040-6090(84)90350-X

Kovacs GJ, Vincett PS, Tremblay C, Pundsack AL (1983) Vacuum deposition onto softenable substrates: formation of novel subsurface structures. Thin Solid Films 101(1):21–40. https://doi.org/10.1016/0040-6090(83)90490-X

Kumar SK, Krishnamoorti R (2010) Nanocomposites: structure, phase behavior, and properties. Annu Rev Chem Biomol Eng 1:37–58. https://doi.org/10.1146/annurev-chembioeng-073009-100856

Lamber R, Wetjen S, Schulz-Ekloff G, Baalmann A (1995) Metal clusters in plasma polymer matrices: gold clusters. J Phys Chem 99(38):13834–13838. https://doi.org/10.1021/jp803934n

Li S, Lin MM, Toprak MS, Kim DK, Muhammed M (2010a) Nanocomposites of polymer and inorganic nanoparticles for optical and magnetic applications. Nano Rev 1:1–19. https://doi.org/10.3402/nano.v1i0.5214

Li D, Li C, Wang A, He Q, Li J (2010b) Hierarchical gold/copolymer nanostructures as hydrophobic nanotanks for drug encapsulation. J Mater Chem 20:7782–7787. https://doi.org/10.1039/c0jm01059f

Massaro A, Spano F, Cingolani R, Athanassiou A (2011) Experimental optical characterization and polymeric layouts of gold PDMS nanocomposite sensor for liquid detection. IEEE Sensors J 11(9):1780–1786. https://doi.org/10.1109/JSEN.2011.2104414

Nanda KK, Maisels A, Kruis FE (2008) Surface tension and sintering of free gold nanoparticles. J Phys Chem C 112(35):13488–13491. https://doi.org/10.1021/jp803934n

Nicolais L, Carotenuto G (2014) Preparation and characterization of metal-polymer nanocomposites. Nanocomposites: in situ synthesis of polymer-embedded nanostructures, 1st edn. John Wiley & Sons Inc, pp 73–95. https://doi.org/10.1002/9781118742655.ch3

Niklaus M, Shea HR (2011) Electrical conductivity and Young's modulus of flexible nanocomposites made by metal-ion implantation of polydimethylsiloxane: the relationship between nanostructure and macroscopic properties. Acta Mater 59: 830–840. https://doi.org/10.1016/j.actamat.2010.10.030

Ozhikandathil J, Badilescu S, Packirisamy M (2012) Gold nanoisland structures integrated in a lab-on-a-chip for plasmonic detection of bovine growth hormone. J Biomed Opt 17(7):077001. https://doi.org/10.1117/1.JBO.17.7.077001

Ozhikandathil J, Khosla A, Packirisamy M (2015) Electrically conducting PDMS nanocomposite using in situ reduction of gold nanostructures and mechanical stimulation of carbon nanotubes and silver nanoparticles. ECS J Solid State Sci Technol 4(10):S3048–S3052. https://doi.org/10.1149/2.0091510jss

Raju D, Bathini S, Badilescu S, Ouellette RJ, Ghosh A, Packirisamy M (2020) LSPR detection of extracellular vesicles using a silver-PDMS nano-composite platform suitable for sensor networks. Enterp Inf Syst 14:532–541. https://doi.org/10.1080/17517575.2018.1526326

Ramesh GV, Porel S, Radhakrishnan TP (2009) Polymer thin films embedded with in situ grown metal nanoparticles. Chem Soc Rev 38(9):2646–2656. https://doi.org/10.1039/b815242j

Ryu D, Loh KJ, Ireland R, Karimzada M, Yaghmaie F, Gusman AM (2011) In situ reduction of gold nanoparticles in PDMS matrices and applications for large strain sensing. Smart Struct Syst 8(5):471–486. https://doi.org/10.12989/SSS.2011.8.5.471

SadAbadi H, Badilescu S, Packirisamy M, Wüthrich R (2012) PDMS-gold nanocomposite platforms with enhanced sensing properties. J Biomed Nanotechnol 8(4):539–549. https://doi.org/10.1166/jbn.2012.1418

SadAbadi H, Badilescu S, Packirisamy M, Wüthrich R (2013) Integration of gold nanoparticles in PDMS microfluidics for lab-on-a-chip plasmonic biosensing of growth hormones. Biosens Bioelectron 44(1):77–84. https://doi.org/10.1016/j.bios.2013.01.016

Scott A, Gupt R, Kulkarni GU (2010) A simple water-based synthesis of au nanoparticle/PDMS composites for water purification and targeted drug release. Macromol Chem Phys 211:1640–1647. https://doi.org/10.1002/macp.201000079

Simpson TRE, Parbhoo B, Keddie JL (2003) The dependence of the rate of crosslinking in poly (dimethyl siloxane) on the thickness of coatings. Polymer 44(17):4829–4838. https://doi.org/10.1016/S0032-3861(03)00496-8

Simpson TRE, Tabatabaian Z, Jeynes C, Parbhoo B, Keddie JL, Al SET (2004) Influence of interfaces on the rates of crosslinking in PDMS coatings. J Polym Sci A Polym Chem 42:1421–1431. https://doi.org/10.1002/pola.20006

Stepanov AL, Khaibullin RI (2004) Optics of metal nanoparticles fabricated in organic matrix by ion implantation. Rev Adv Master Sci 7:108–125

Zhang Q, Xu JJ, Liu Y, Chen HY (2008) In-situ synthesis of poly(dimethylsiloxane)-gold nanoparticles composite films and its application in microfluidic systems. Lab Chip 8(2): 352–357. https://doi.org/10.1039/b716295m